Torsion−Vibration Coupling in Methanol: Diabatic Behavior in the CH Overtone Region

David S. Perry

Department of Chemistry, The University of Akron, Akron, Ohio 44315-3601

Received: September 10, 2007; In Final Form: October 22, 2007

Through a fit to methanol CH overtone data, a previously developed 4-dimensional torsion−vibration Hamiltonian is extended to high CH stretch excitation as well as to high torsional excitation. The strength of the torsion−vibration coupling is found to increase with CH stretch excitation. Systematic patterns of near degeneracy (3-, 4-, and 6-fold) are found in different regions of quantum number space. In the region of the CH fundamentals, an approximate adiabatic separation of the torsion (slow degree of freedom) from the CH stretches (fast degrees of freedom) accounts for the pattern of the energy levels and for the signs of the torsional tunneling splittings. For the higher CH overtones ($v_{CH} \geq 4$), a diabatic representation accounts for the torsional structure obtained from the fully coupled calculation and for certain trends found in the pattern of the energy levels.

I. Introduction

Large amplitude nuclear motion challenges the traditional theory of molecular vibrations, which relies on the assumption of small amplitude vibrational motion relative to a fixed reference geometry. Instead of point group theory, we now need to use permutation−inversion group theory to treat the symmetry of the Hamiltonian.[1] Jon Hougen has shown that in molecules with 3-fold internal rotors, such as methanol, the symmetries of the normal modes are not unique.[2]

The adiabatic approximation provides one means of defining normal modes in the presence of large amplitude motion. In the adiabatic treatment of methanol by Fehrensen et al.,[3] the 11 small amplitude vibrations are solved at each torsional angle, and then the torsional motion is solved in the effective potential of the other vibrations. Through the use of geometric phase, this approach provides a general method of predicting which vibrations will have inverted torsional tunneling splittings. In methanol, several vibrations, including the ν_2 and ν_9 CH stretches, have torsional tunneling splittings with the E level below the A level, rather than A below E as in the vibrational ground state.[4−9]

The reduced dimensional (4-D) Hamiltonian of Wang and Perry,[4] which included only the torsion and the three CH stretches, was able to account for the inverted torsional tunneling splittings of the ν_2 and ν_9 vibrations without the use of an approximate separation of the degrees of freedom. That model includes a local-mode treatment of the CH stretches, with a harmonic frequency ω and a local−local coupling parameter λ. For the torsional motion, the ground-state torsional potential is used. The model has a single torsion−vibration coupling parameter μ, which reflects the fact that the harmonic frequency for the CH anti to the OH bond is higher than for the CH gauche to it. Clasp and Perry[10] applied the adiabatic approximation to obtain approximate solutions to the 4-D Hamiltonian so that they could be compared to the fully coupled solutions previously obtained. The adiabatic solutions have the correct inverted torsional tunneling of the ν_2 and ν_9 vibrations but do not show the 4-fold near degeneracies obtained from the fully coupled calculation at higher torsional energies.

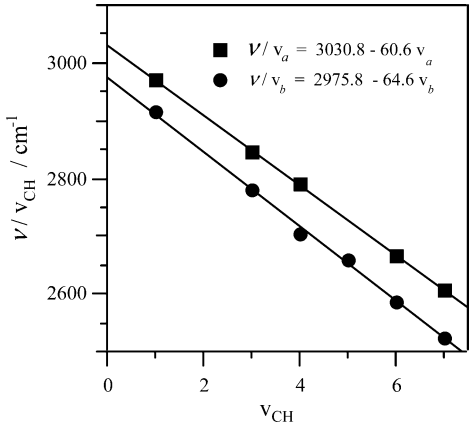

Figure 1. Birge−Sponer plots for CH overtones of methanol. The overtone data are from ref 13 for $v_{CH} = 3-5$ and ref 14 for $v_{CH} = 6$, 7. The points for $v_{CH} = 1$ are hypothetical local CH stretch frequencies as calculated in ref 13 from the high-resolution CH stretch fundamental band origins. The lines are fits of the data points.

The bifurcation analysis of Kellman and co-workers[11,12] has shown that new kinds of vibrational modes can be born at high excitation energies. Examples include the normal to local transition found in the overtone spectra of hydride stretches and the several new modes found in acetylene when different combinations of the cis and trans bends are highly excited. In methanol in absence of torsional excitation, ν_2 and ν_9 are best treated as distinct normal modes (A_1 and A_2 symmetries in the G_6 molecular symmetry group), but at high torsional excitation, our model calculations[10] have shown that they coalesce into a single, doubly degenerate, E-type normal mode that combines with nearly free internal rotation. In this paper, we extend our 4-D model Hamiltonian to the CH overtone region to explore the new kinds of nuclear motion that occur in this torsional molecule when the CH bonds are excited to large amplitude vibrations.

In section II, the extended Hamiltonian and the computational methods are developed. In section III, the energy level patterns

* To whom correspondence should be addressed. E-mail: dperry@uakron.edu. Phone: (330) 972-6825.

10.1021/jp077269q CCC: $40.75
Published on Web 12/23/2007

TABLE 1: Model Parameters

parameter	value in cm^{-1}	std dev
ω	3060.74	1.34
ωx	−63.63	0.66
μ	15.54	0.87
μx	1.53	0.43
λ	−42.10	a
F	27.65	b
V_3	373.54	b
V_6	−0.8	b

[a] Held constant at the value from ref 4. [b] Held constant at the values from ref 22.

and new vibrational modes are characterized with the aid of the adiabatic and diabatic approximations.

II. Computational Method

A. The Model Hamiltonian. In our previous work,[4,10] the vibrational parameters of the 4-D Hamiltonian, ω, λ, and μ, were fit to the band origins and the torsional tunneling splittings of the three CH fundamentals, while the torsional parameters, F, V_3, and V_6, were held fixed at the values obtained for the vibrational ground state. However, it is useful to note that a good approximation to the best fit values of ω, λ, and μ can be obtained only from the three CH band origins (ν_2, ν_3, ν_9). Because the torsion−vibration coupling μ derives from the fact that the CH stretch force constant is larger for the CH bond anti to the OH than for the CH bonds gauche to it, the frequency difference between the two asymmetric CH stretches, $\nu_2-\nu_9$, can be used to determine the value of μ. The difference between the symmetric stretch and the average of the asymmetric stretches, $\nu_3 - (\nu_9 + \nu_2)/2$, determines the local−local coupling λ, and the average of the three band origins determines the local CH frequency ω. The calculated torsional tunneling splittings agreed well with those from high-resolution spectra of the three fundamentals[4] and served mainly as a check on the validity of the model Hamiltonian.

To extend the Hamiltonian to high CH stretch excitation, we use the overtone data[13,14] summarized in the Birge−Sponer plots of Figure 1. The overtone data for $\upsilon_{CH} = 3-7$ fall in two straight lines in Figure 1, which is the behavior expected[14] for a molecule with two different CH stretch chromorphores, each giving rise to overtone spectra as if it were an isolated diatomic molecule. In methanol, the unique CH, anti to the OH, is labeled "*a*", and the two nonunique CH bonds gauche to the OH are labeled "*b*". Even though the $\upsilon_{CH} = 3-5$ spectra were recorded for jet-cooled methanol with a 5−10 K rotational temperature, no torsional or rotational structure was observed in these bands. It is likely that intramolecular vibrational redistribution (IVR) in combination with congested torsion−rotation structure has resulted in the smoothly broadened features found in these spectra. Despite the disappointing lack of rotationally resolved data, the CH overtone spectra still do contain precise information about the torsion−vibration coupling when the CH stretch is highly excited. At each overtone level, the splitting $\upsilon_{CH}\nu_a - \upsilon_{CH}\nu_b$ measures the energy difference between v_{CH} quanta in a CH bond anti to the OH and v_{CH} quanta in a CH bond gauche to it. That is, the splitting reflects the torsional angle dependence of the energy of a CH bond with υ_{CH} quanta, and it is thus a measure of the torsion−vibration coupling at that overtone level. The splitting $7\nu_a - 7\nu_b$ is 570 cm^{-1}, large enough that $7\nu_a$ and $7\nu_b$ are well separated even in room-temperature photoacoustic spectra.[14]

The local-mode notation, ν_a and ν_b, does not apply in the fundamental ($\upsilon_{CH} = 1$) region because the local−local coupling λ splits the three degenerate local CH fundamentals into the normal modes ν_3 and $\{\nu_2, \nu_9\}$. However, since the fundamentals have been fit with our local-mode Hamiltonian, we are able to use the model to extract hypothetical local-mode frequencies for the ν_a and ν_b fundamentals,[13] and these are included in Figure 1.

The most obvious next step is to determine the anharmonicity of the local CH stretches from the slopes in Figure 1. However, the slopes of the two lines are different, which means that, in order to use a common anharmonicity, ωx, for all three CH bonds, we also need to include the anharmonicity, μx, of the torsion−vibration coupling.

With these extensions, the 4-D model Hamiltonian becomes

$$H = H_{str} + H_{l-l} + H_{tors} \quad (1)$$

where, in eq 1, the CH stretch Hamiltonian H_{str} is expanded in a Fourier series in the torsional angle γ

$$H_{str} = H_{str}^{(0)} + H_{str}^{(1)} + ... \quad (2)$$

Superscript (0) indicates constant terms and (1) indicates terms in cos γ, etc.

$$H_{str}^{(0)} = \omega\left(\upsilon_1 + \frac{1}{2} + \upsilon_2 + \frac{1}{2} + \upsilon_3 + \frac{1}{2}\right) + \omega x\left[\left(\upsilon_1 + \frac{1}{2}\right)^2 + \left(\upsilon_2 + \frac{1}{2}\right)^2 + \left(\upsilon_3 + \frac{1}{2}\right)^2\right] \quad (3)$$

and

$$H_{str}^{(1)} = 2\mu\left[\left(\upsilon_1 + \frac{1}{2}\right)\cos\gamma + \left(\upsilon_2 + \frac{1}{2}\right)\cos\left(\gamma - \frac{2\pi}{3}\right) + \left(\upsilon_3 + \frac{1}{2}\right)\cos\left(\gamma + \frac{2\pi}{3}\right)\right] + \mu x\left[\left(\upsilon_1 + \frac{1}{2}\right)^2\cos\gamma + \left(\upsilon_2 + \frac{1}{2}\right)^2\cos\left(\gamma - \frac{2\pi}{3}\right) + \left(\upsilon_3 + \frac{1}{2}\right)^2\cos\left(\gamma + \frac{2\pi}{3}\right)\right] \quad (4)$$

The requirement that the Hamiltonian be totally symmetric (A_1) in the molecular symmetry group (G_6) determines the linear combinations and phase angles in eq 4. The local−local coupling term is

$$H_{l-l} = \lambda(a_1^{+}a_2 + a_1a_2^{+} + a_1^{+}a_3 + a_1a_3^{+} + a_2^{+}a_3 + a_2a_3^{+}) \quad (5)$$

where a_i^{+} and a_i are the ladder operators for harmonic vibrations on the CH bond *i*. The ground state torsional Hamiltonian is

$$H_{tors} = F\mathbf{j}_\gamma^{\,2} + \frac{V_3}{2}(1 - \cos 3\gamma) + \frac{V_6}{2}(1 - \cos 6\gamma) \quad (6)$$

To determine values of ω, ωx, μ, and μx, we fit eqs 3 and 4 to the data points in Figure 1. For the fit, we hold γ fixed at 0 for the unique hydrogen and at $2\pi/3$ for the nonunique hydrogens. The transition frequencies are therefore fit to the expression

$$\nu = \omega(\upsilon_a + \upsilon_b) + \omega x(\upsilon_a^{\,2} + \upsilon_a + \upsilon_b^{\,2} + \upsilon_b) + \mu(2\upsilon_a - \upsilon_b) + \mu x(2(\upsilon_a^{\,2} + \upsilon_a) - (\upsilon_b^{\,2} + \upsilon_b)) \quad (7)$$

Because the band origins of the fundamentals were determined from high-resolution spectroscopy, they are much more accurately known than the overtone band origins and were therefore are given much larger weights. Weights 250 times larger were sufficient to ensure that the parameters in Table 1

reproduce the previous model calculations[4] for $v_{CH} = 1$ precisely. The new values of ω and μ are related to the previously used values[4,10] (noted here as $\omega_{1\leftarrow0}$ and $\mu_{1\leftarrow0}$) by the equations $\omega_{1\leftarrow0} = \omega + 2\omega x = 2933.48\ cm^{-1}$ and $\mu_{1\leftarrow0} = \mu + 2\mu x = 18.6\ cm^{-1}$.

B. Basis Set for Fully Coupled Calculations. The basis set used for the calculation is the product basis of a harmonic oscillator on each CH bond ($v_i = 1, 2, 3$) times a free internal rotor function

$$|v_1, v_2, v_3, m\rangle = |v_1\rangle|v_2\rangle|v_3\rangle|m\rangle$$
$$= (2\pi)^{-1/2} e^{im\gamma}|v_1\rangle|v_2\rangle|v_3\rangle,\ m = 0, \pm 1, \pm 2, \ldots \quad (8)$$

The model Hamiltonian conserves the polyad number $v_{CH} = v_1 + v_2 + v_3$, and the number of CH vibrational states in each polyad from $v_{CH} = 0-6$ is 1, 3, 6, 10, 15, 21, and 28. The free rotor basis is truncated at $|m| \leq m_{max} = 12$, which for the $v_{CH} = 6$ gives a polyad of $25 \times 28 = 700$ torsion−vibration states. Our previous studies of the scaling behavior of this Hamiltonian[10] have shown that with $m_{max} = 12$ the torsional eigenfunctions with $m^* \leq 6$ converge to within about 0.01% and those with $m^* \leq 9$ to within about 0.3%, where m^* denotes the free internal rotor basis function that has the greatest contribution to a given eigenfunction.

C. Approximate Adiabatic and Diabatic Calculations. The purpose of the present approximate calculations is to provide a point of reference that will help us to understand the fully coupled results. We would also like to find the domain of applicability of the approximate methods. In the present situation, we have a limited dimensional Hamiltonian, and fully coupled calculations are easily accomplished on a small computer. However, full-dimensional fully coupled calculations on methanol and other systems of interest are not yet tractable without some sort of separation of variables. We will show below that different kinds of motion occur in different regions of quantum number space and that the applicability of a particular approximate method can help to characterize that motion.

Our approach to implementing an approximate adiabatic solution has been described in detail previously.[10] Briefly, the vibrational motion is solved in the harmonic basis at each torsional angle, γ. Then the vibrational eigenvalues taken as a function of γ are used as the effective potentials, and the torsional motion is solved in these potentials. For some CH vibrational states, such as the ν_2 and ν_9 fundamentals, a geometric phase of -1 is accumulated as γ goes from 0 to 2π. In these cases, the Schroedinger equation for the 1-D torsional motion is solved with 4π boundary conditions, and the symmetries of the torsional eigenfunctions are selected to ensure that the total wavefunction (vibrational part × torsional part) remains invariant when $\gamma \rightarrow \gamma + 2\pi$. This means that, when the geometric phase is -1, the torsional angular momentum has half-integer values, $m = \pm 1/2, \pm 3/2, \pm 5/2, \ldots$. First-order corrections can be applied to the zeroth-order (or crude) adiabatic approximation described above to obtain the adiabatic limit. In previous work on this Hamiltonian,[10] we have found that the first-order corrections shifted the eigenvalues somewhat to higher energy but did not affect the pattern of near degeneracies or ordering of the levels. Accordingly, only zeroth-order adiabatic calculations are presented in this paper.

One of the consequences of the adiabatic approximation is that the character of the vibrational wavefunctions changes as a function of the torsional angle. Suppose that in the present case we had a vibration (such as ν_2) in which most of the CH stretch amplitude was concentrated in the CH bond anti to the OH bond. When the torsional angle changes by 120°, a different CH bond will be anti to the OH bond, and the vibrational excitation moves to the new anti CH bond. In the lower polyads, such as $v_{CH} = 1$, the vibrational amplitude moves slowly and smoothly between the different CH bonds as the torsional angle is varied;[10] however, in the higher polyads, we find that the vibrational character of the local CH overtones can change abruptly in the vicinity of an avoided crossing.

The counterpoint to the adiabatic approximation is the diabatic approximation in which potential curves of the same symmetry may cross. As in the case of electronic spectroscopy, the diabatic approach would seem to be called for when the adiabatic curves have a very narrowly avoided crossing. In such cases, we implement the diabatic approximation by interpolating the adiabatic curves across the avoided crossing to form diabatic curves that actually cross. The 1-D torsional motion is then solved in the diabatic potential.

III. Results and Discussions

A. Fully Coupled Solutions. The lowest calculated eigenvalues obtained for each polyad are displayed in Figure 2. A number of diagnostics were used to characterize the eigenfunctions, including symmetry (A_1, A_2, or E), torsional angular momentum ($m_{rms} = (\langle m^2 \rangle)^{1/2}$), and local CH stretch character. The latter is the probability that all of the CH stretch excitation will reside on a single bond and is calculated for the v_{CH} polyad eigenfunction ψ_i as

$$L_i = \sum_{m=-m_{max}}^{m_{max}} |\langle \psi_i | v_{CH}, 0, 0, m\rangle|^2 + |\langle \psi_i | 0, v_{CH}, 0, m\rangle|^2 + |\langle \psi_i | 0, 0, v_{CH}, m\rangle|^2 \quad (9)$$

The local CH stretch character L_i is of most interest here because it is responsible for the dominant oscillator strength in overtone spectra. Although there is some mixing of local and nonlocal states, an inspection of Figure 2 shows that many local states with $L_i \approx 1$ can be identified. Among such local states, one can see systematic trends of increasing m_{rms} with energy above the lowest state in each polyad. The remainder of this paper focuses on the properties of these local states.

Among the local states, there are systematic patterns of near degeneracies (Figure 2), which vary with the amount of torsional energy and with the amount of CH stretch energy in the molecule. In the CH stretch ground state ($v_{CH} = 0$) at low torsional energy, there are only the singly degenerate A_1 and A_2 levels and the doubly degenerate E levels required by the G_6 molecular symmetry group (isomorphic to C_{3v}). At high torsional energy, the torsion becomes nearly free internal rotation, and pairs of A_1 and A_2 levels approach degeneracy. In this limit, the internal rotations in the positive and negative directions become uncoupled, the torsional angular momentum m becomes a good quantum number, and the symmetry of the internal rotation can be treated approximately with the point group $C\infty_v$.

In the polyad $v_{CH} = 1$, we have the complication of the CH stretch motion, which, when coupled to the torsion, gives inverted torsional tunneling for the ν_2 and ν_9 fundamentals. As for $v_{CH} = 0$, the lowest torsional states in the $v_{CH} = 1$ polyad show only the single and double degeneracies required by the A_1, A_2, and E species of the G_6 group. At higher torsional energies, A_1 and A_2 pairs approach degeneracy and also the ν_2

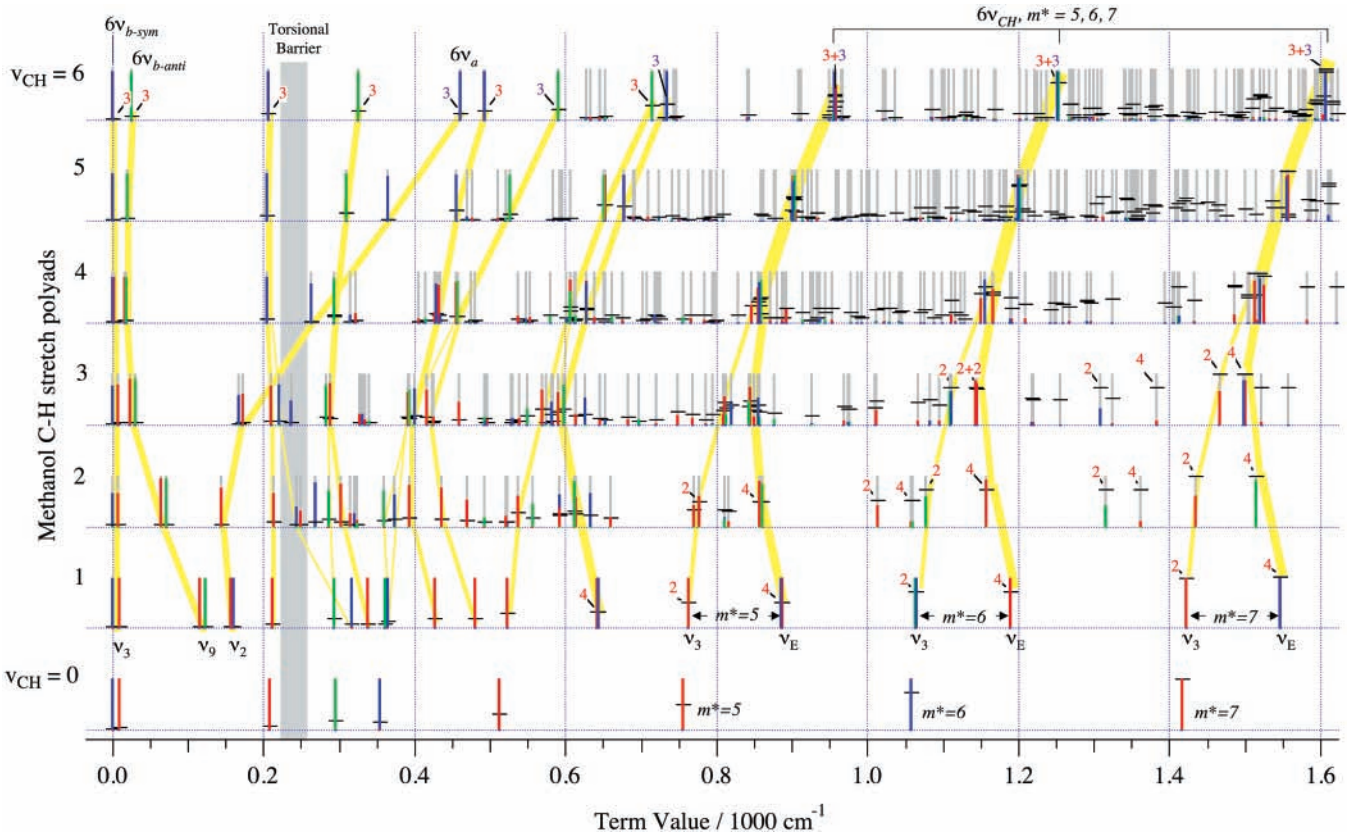

Figure 2. Fully coupled computed torsion−vibration term values for methanol. In each CH stretch polyad, the term values are given relative to the lowest energy term in that polyad. Colors indicate the symmetries of each eigenstate (blue = A_1, green = A_2, red = E), and the portion of each line that is colored indicates its local character L_i in the range from 0 to 100%. The remainder of each line is gray, and the states that are all gray have little, if any, local character. The position of the bar (−) on each eigenstate indicates the value of the torsional angular momentum m_{rms} on a scale from 0 (bottom) to 7 (top). The yellow lines trace the correlation of states with high L_i from one polyad to the next. Arabic numerals indicate the degeneracy of some levels that are degenerate within the width of the printed lines.

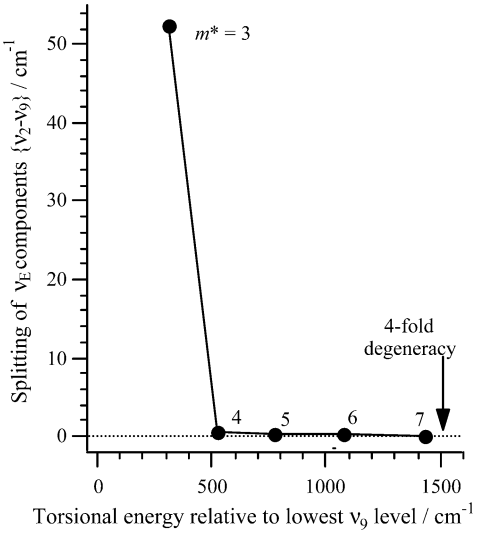

Figure 3. Approach of the ν_2 and ν_9 vibrations to a degenerate ν_E vibration as the torsional energy is increased.

and ν_9 vibrations converge to give systematic 2- and 4-fold degeneracies. Figure 3 shows that the convergence of ν_2 and ν_9 to an E-type degenerate asymmetric CH stretch appears to be nearly complete by $m^* = 4$, at about 2× the torsional barrier height. Here m^* indicates the torsional angular momentum of the free rotor basis function making the largest contribution to a given eigenfunction.

When the CH stretch excitation is increased while the torsional energy is kept low, different changes in the pattern of the energy levels take place. The yellow correlation lines in Figure 2 show that ν_2 correlates to ν_a while ν_9 and ν_3 converge to the ν_b. Since there are two equivalent gauche hydrogens, the symmetrized eigenstates in the usual local-mode picture[15] will be the symmetric and antisymmetric combinations of these two vibrations, ν_{b-sym} and ν_{b-anti}, with ν_3 correlating to ν_{b-sym} and ν_9 to ν_{b-anti}. As the overtone level increases, the splitting $\upsilon_{CH}\nu_{b-anti}-\upsilon_{CH}\nu_{b-sym}$ is expected to decrease rapidly to zero because the coupling of these states requires the exchange of an increasing number of vibrational quanta by way of nonresonant intermediate states.[15] Figure 4b and the leftmost pair of yellow lines in Figure 2 show that this is not the case here. We find that the splitting $\upsilon_{CH}\nu_9-\upsilon_{CH}\nu_3$ decreases rapidly from $\upsilon_{CH} = 1-3$ and reaches a minimum at $\upsilon_{CH} = 4$. To higher υ_{CH}, the splitting (now more appropriately notated as $\upsilon_{CH}\nu_{b-anti}-\upsilon_{CH}\nu_{b-sym}$) turns around and begins to increase slowly.

The approach of the overtones $\upsilon_{CH}\nu_3$ to the local-mode limit as υ_{CH} increases from 2 to 6 is shown in Figure 4c. The local character L_i (eq 9) appears to increase asymptotically toward 1.0 for the higher overtones. The difference $1 - L_i$ represents the extent that local−local combinations contribute to the computed eigenfunctions. At $\upsilon_{CH} = 2$, the possible local−local combinations are $|1,1,0\rangle$, $|1,0,1\rangle$, and $|0,1,1\rangle$, and at higher υ_{CH}, there are an increasing number of possible local−local combinations. The reason for the declining contribution of the local−local combinations as υ_{CH} increases is the increasing anharmonic shift of the local basis functions $|\upsilon_{CH},0,0\rangle$ relative to the nearest local−local combination $|\upsilon_{CH} - 1,1,0\rangle$.

The changes in the E−A torsional tunneling splittings with υ_{CH} are shown in Figure 4a. The magnitude of the torsional

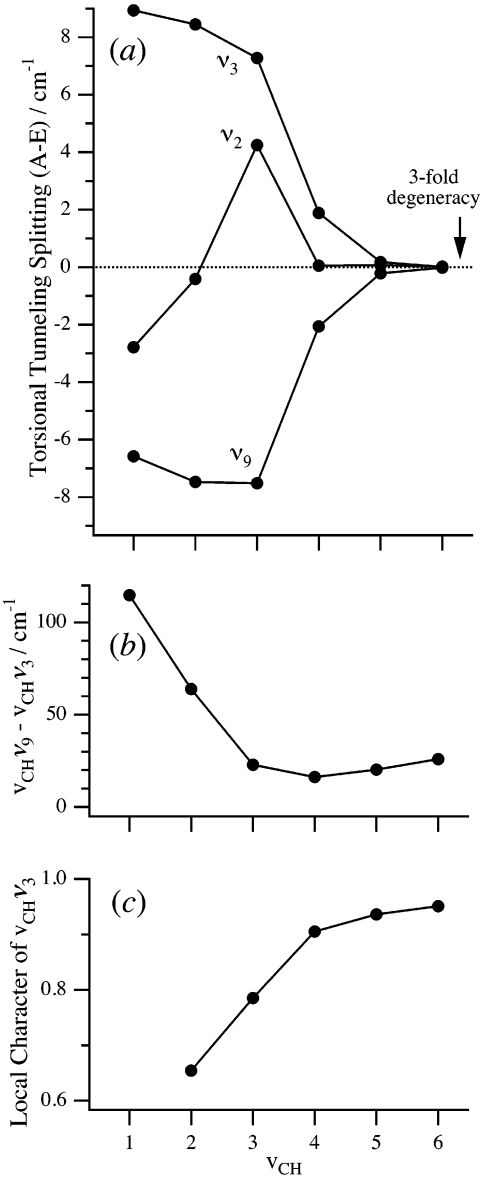

Figure 4. Changes in three quantities as the local CH stretch is excited: (a) the E−A torsional tunneling splittings, (b) the splitting between the ν_3 and ν_9 overtones, which correlate to $\nu_{b-\mathrm{sym}}$ and $\nu_{b-\mathrm{anti}}$, respectively, at high CH excitation, and (c) the local character of the ν_3 overtones.

tunneling splitting for each of the overtone vibrations decreases sharply between $v_{CH} = 3$ and 4 and then appears to approach asymptotically to zero for higher v_{CH}. That is, torsional tunneling appears to be quenched for the high-lying local CH stretch excited states. From Figure 2, one can see that all of the local states in the $v_{CH} = 6$ polyad have 3-fold or higher near degeneracies. It is interesting to note that the tunneling splitting of the ν_2 overtones actually changes sign before converging to zero. Together the three panels of Figure 4 show a change of behavior near $v_{CH} = 4$. Such a change is expected for the transition from normal to local behavior for hydride overtones. We are left with two questions about the behavior of this torsional molecule: (i) Why is torsional tunneling rapidly quenched above $v_{CH} = 4$? (ii) Why does the splitting $v_{CH}\nu_{b-\mathrm{anti}} - v_{CH}\nu_{b-\mathrm{sym}}$ begin to increase above $v_{CH} = 4$?

Before attempting to answer these questions, we will look at the behavior of the high CH overtone local states at high torsional energy. There is a convergence to 6-fold degeneracy that may be followed as a function of CH stretch excitation

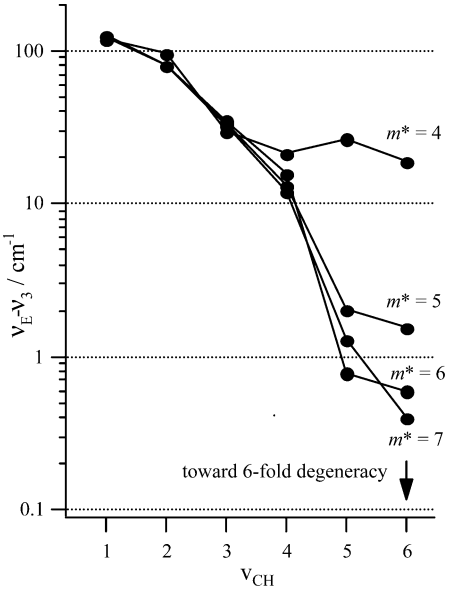

Figure 5. Convergence of ν_3 and ν_E to degeneracy with increasing CH stretch excitation, shown for four different amounts of internal rotation.

(Figure 5 and the yellow correlation lines in the right part of Figure 2). At high internal rotation energy in $v_{CH} = 1$, the near degeneracies of the ν_3 and ν_E vibrations are 2 and 4, respectively. As v_{CH} increases, ν_3 and ν_E are transformed into three identical local modes, which we call ν_{CH}, and this results in 6-fold near-degeneracy. The 6-fold degeneracies can be understood as free internal rotation (2-fold degenerate) combined with the overtones of ν_{CH} (triply degenerate).

The convergence to 6-fold degeneracy may also be followed as a function of torsional excitation (moving left to right across the top panel of Figure 2). For $v_{CH} = 6$, the 3-fold degenerate local states converge in pairs to 6-fold degenerate sets. The approach to the free internal rotor limit is qualitatively different than in the CH ground state. For $v_{CH} = 0$, the torsional tunneling splitting increases from a small value (9 cm^{-1}) until it becomes the spacing between the free internal rotor levels (bottom panel of Figure 2). For $v_{CH} = 6$, the torsional tunneling splitting (E−A) of the local states remains very small ($\sim$0.01 cm^{-1}) as the torsional energy is increased. Instead, the splitting between the $6\nu_{b-\mathrm{anti}}$ and the $6\nu_{b-\mathrm{sym}}$ states increases with torsional excitation until it is equal to the free internal rotor spacing. The resulting $6\nu_b$ levels (alternating sym and anti) then converge with the $6\nu_a$ levels as the torsional energy is increased. For $v_{CH} = 4$ and 5, the behavior is similar although the convergence to 6-fold degeneracy is not as complete. This leads us to ask a third question: (iii) In the higher polyads, why does torsional excitation not increase the E−A torsional tunneling splittings? To answer these three questions, we will employ approximate adiabatic and diabatic solutions for the same Hamiltonian.

B. Adiabatic and Diabatic Approximate Solutions. The first step in the adiabatic approach is to solve the CH vibrational problem at each torsional angle, thereby to obtain the effective potentials in which the torsional motion can be solved. The effective torsional potentials for $v_{CH} = 1$ are shown in Figure 6a. Each of the three adiabatic potentials (ν_3, ν_9, and ν_2) retains the 3-fold symmetry and the approximate amplitude of the ground state torsional potential. The curves do not cross, and there are no narrowly avoided crossings. The vibrational character changes gradually with γ so that, when γ changes by 120°, the vibrational amplitude moves between different CH bonds. The torsional eigenfunctions and eigenvalues for each

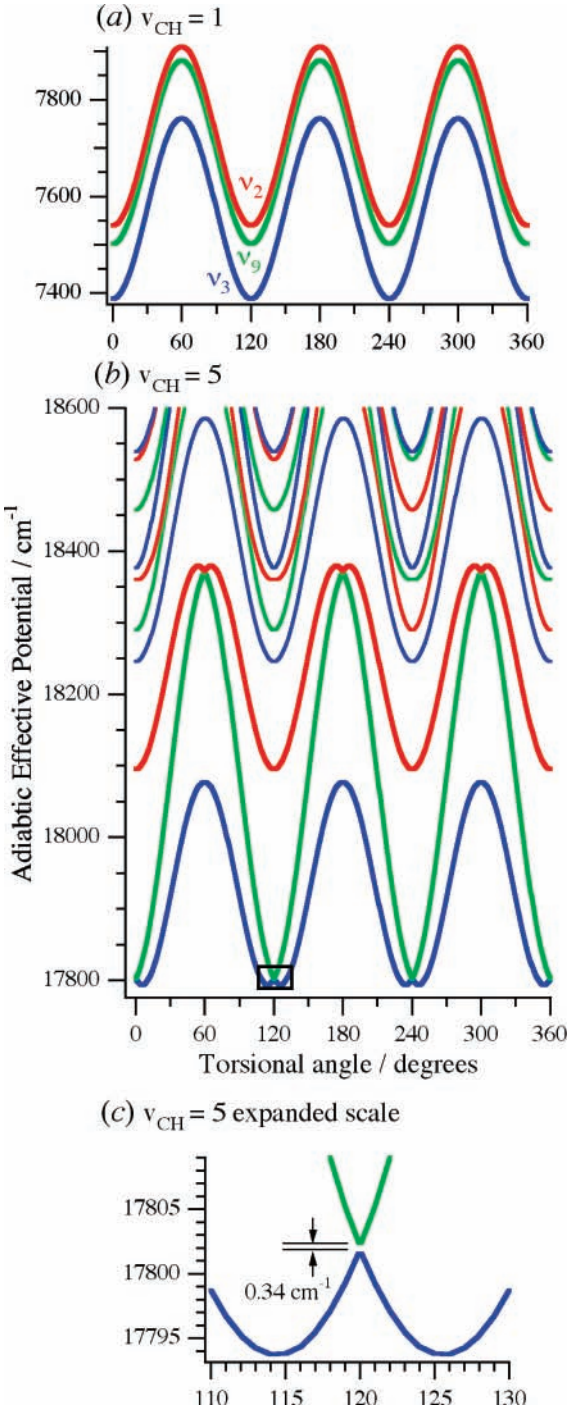

Figure 6. Adiabatic potentials for (a) $v_{CH} = 1$ and (b) $v_{CH} = 5$. The highlighted avoided crossing in (b) is shown on an expanded scale in (c).

of the three effective potentials have been previously reported.[10] Qualitatively correct torsional tunneling splittings are obtained for the lowest torsional levels on each potential provided that proper account is taken of geometric phase.

The effective potentials for the $v_{CH} = 5$ polyad are shown in Figure 6b. The lowest three curves are approximately described as linear combinations of the three local states, $|5,0,0\rangle$, $|0,5,0\rangle$, and $|0,0,5\rangle$, and the higher curves are mixtures of the local−local combination basis states. These adiabatic potentials all have 3-fold symmetry, but now their shapes and amplitudes are very different from the ground-state torsional potential. In fact, there are 6 very narrowly avoided crossings involving the three lowest curves, one of which is shown on an expanded scale in Figure 6c. The narrowly avoided crossings suggest the appropriateness of the diabatic approximation.

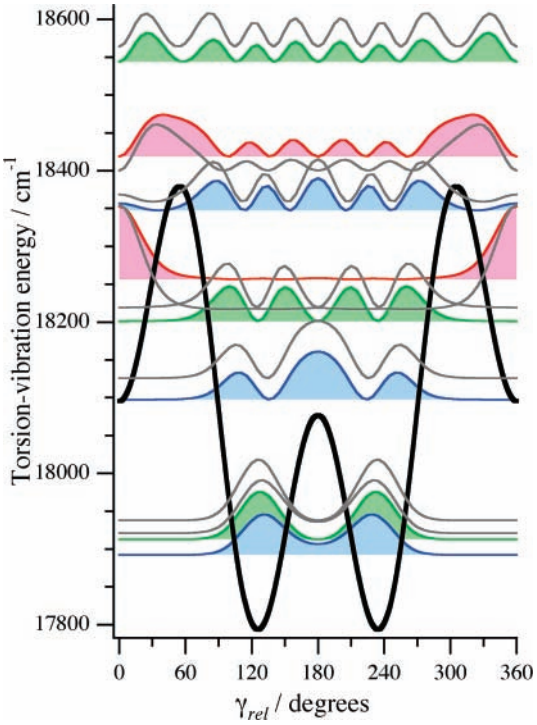

Figure 7. For the $v_{CH} = 5$ polyad, the diabatic effective potential (C_s symmetry) is shown in black. The abscissa is the torsional angle relative to the local CH stretch, defined such that $\gamma_{rel} = 0$ when the OH bond is anti to the excited CH bond. The energies of the fully coupled eigenfunctions and the torsional probability distributions for the local part of those eigenfunctions are represented in color: eigenfunctions localized in the anti conformation are shown in red; the others are shown by their symmetry in C_s: blue for A′ and green for A″. The energies and torsional probability distributions calculated in the diabatic approximation are shown in gray.

Accordingly, a set of three diabatic potentials were formed by smoothly interpolating across the small gaps between the lowest three adiabatic curves in Figure 6b. Along each of the diabatic curves, the CH stretch excitation remains localized on a particular CH bond. The three diabatic potentials all have the same form but are shifted one from the other by ±120°. In fact, the three diabatic curves are identical if they are plotted (Figure 7) against the torsional angle γ_{rel} of the OH bond relative to the CH bond that is excited. Unlike the adiabatic curves, the diabatic potential curves are not 3-fold symmetric. The torsion−vibration coupling (eq 4) causes the energy of the local vibration $|5,0,0\rangle$, and hence the energy of the diabatic potential curves, to be higher when the excited CH bond is anti to the OH bond ($\gamma_{rel} = 0°$) than when it is gauche to it ($\gamma_{rel} \approx 120, 240°$).

We solved the 1-dimensional torsional motion in these diabatic potentials to obtain torsional eigenfunctions and energies represented in Figures 7 and 8. In Figure 8, the adiabatic and diabatic approximate energies are compared to the exact (fully coupled) energies for the $v_{CH} = 5$ polyad. As noted above, the fully coupled calculation gives 3-fold near degeneracies. In each triplet, an A_1 or A_2 level is nearly degenerate with an E level. The residual splittings in the exact calculation are so small that the A and E levels appear to be exactly degenerate in Figure 8. In the diabatic calculation, the triplets are precisely degenerate because the three diabatic potentials are equivalent. In contrast, the adiabatic energies in Figure 8 do not show a pattern of systematic 3-fold degeneracies.

The torsional probability distributions for the exact and diabatic calculations are compared in Figure 7. Since the fully

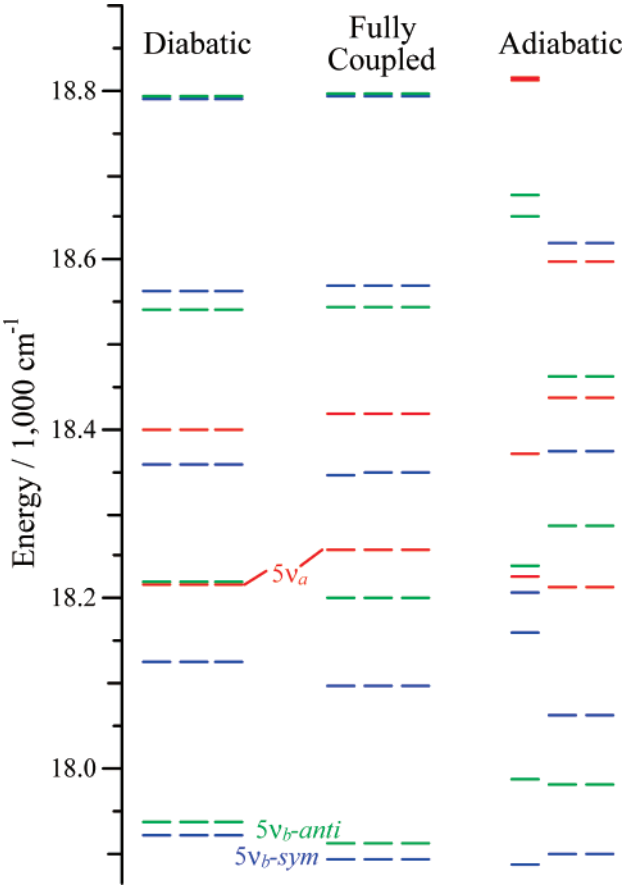

Figure 8. For the $v_{CH} = 5$ polyad, the fully coupled energies of the local CH stretch states are shown using the color scheme of Figure 7, and the approximate diabatic energies are shown with the same color scheme. Adiabatic energies, calculated for the lowest three adiabatic potentials shown in Figure 6, are shown using the color scheme of Figure 6. For the fully coupled energies, the left-hand member of each triplet is an A_1 or A_2 state (in G_6), and the two left-hand members represent the degenerate E levels. For the adiabatic energies, the same convention is used, but the diabatic energies are exactly degenerate by construction and the symmetries in G_6 are not defined.

coupled probability distributions are defined in 4 dimensions, it is necessary to project them onto a single torsional coordinate in a way that is directly comparable to the diabatic calculation. For this purpose, we project out the local portion of the wavefunctions ($L_i \approx 90\%$ for $v_{CH} = 5$) and calculate the probability distribution of that portion as a function of the relative torsional angle, γ_{rel}. Qualitatively, the probability distributions for the local part of the exact wavefunctions agree well with the diabatic calculation.

Although the qualitative agreement is good, there are some quantitative differences between the diabatic and exact calculations. For the probability distributions, the difference is most evident for the torsional function that is localized near the anti conformation and has an energy just above the top of the torsional barrier (uppermost red curve in Figure 7). Over the range plotted in Figure 8, the diabatic energies are on average 3 cm^{-1} too high and the root-mean-square error of the diabatic energies is 20 cm^{-1}. We have not attempted to formulate correction terms in the diabatic representation, but as for the adiabatic representation, there would be first order corrections diagonal in the diabatic basis and higher order corrections that would represent both the mixing of local and nonlocal CH stretches and the contribution of adiabatic paths at the curve crossings.

The qualitative success of the diabatic solution provides an answer to question (i) above. For torsional tunneling to occur and to thereby produce tunneling splittings between the A and E levels, the system must follow the adiabatic path. For example, in the $v_{CH} = 5$ polyad, the adiabatic torsional tunneling path (parts b and c of Figure 6) requires five quanta of CH stretch vibration localized on one CH bond to jump to the next over a very small range of the torsional angle (1° or less). The narrowly avoided crossings of the adiabatic curves indicate that the diabatic curves are only weakly coupled. In the diabatic representation, to effect the transfer of 5 quanta of CH stretch from bond 1 to bond 2 would require a coupling term tenth-order in the ladder operators, such as $(a_1)^5(a_2^+)^5$. As was found in the calculation of splitting of anti and sym combinations of local-mode overtone states,[15,16] such high-order couplings are expected to be weak and to decrease rapidly as the order increases. The weak coupling of the diabatic states results in slow tunneling and very small E−A splittings.

Question (ii) above asked why the present calculation is an exception to the expected convergence of the anti and sym combinations of the ν_b local-mode overtones. The answer can be found in the diabatic torsional potential in Figure 7. Because $\nu_a > \nu_b$, the diabatic potential at $\gamma = 0°$ is greater than at $\gamma = 120°$. As the overtone level increases, the barrier (at $\gamma = 180°$) between the two equivalent gauche conformations decreases slightly, which in turn increases the tunneling rate between the two gauche wells as measured by the splitting $v_{CH}\nu_{b-anti} - v_{CH}\nu_{b-sym}$.

The E−A torsional tunneling rate does not increase with torsional excitation (question (iii)) because torsional tunneling in that context involves the hopping of the CH vibrational excitation from one CH bond to another, and that hopping is entirely quenched in the diabatic limit. We have instead the torsional dynamics on three identical diabatic potentials such as shown in Figure 7. We do have tunneling between the two gauche conformations on that potential, but it is tunneling of a different sort. It is torsional tunneling *relative to the location of the CH stretch excitation* and does not involve movement of CH stretch amplitude from one bond to the next.

C. Comparison with Experiment. The limitations of the present model must be kept in mind when comparing the results, whether exactly computed or approximate, to experimental spectra. Methanol is a 12-dimensional torsion−vibration problem, and many of the other degrees of freedom will interact on some time scale with the four degrees of freedom considered here. There is a strong 1:2 CH stretch−bend resonance interaction in the CH fundamental region that also affects some states in the higher polyads as well. The IRLAPS spectrum the $v_{CH} = 2$ region[13] (Figure 9) contains several partially resolved bands, which have been tentatively assigned by Hänninen and Halonen[17] as CH normal-mode combinations interacting with HCH bends (ν_4, ν_5, and ν_{10}). For that calculation, Hänninen and Halonen derived anharmonic resonance terms up to quartic from their ab initio surface but did not include torsional tunneling. The $v_{CH} = 2$ polyad lies in the transition region between the normal-mode behavior of the fundamentals ($v_{CH} = 1$) and the onset of local-mode behavior for the higher polyads. Because of this and because of the complexities resulting from the stretch−bend resonance, we did not use the $v_{CH} = 2$ spectra in developing the present model, but we are able to calculate transition frequencies in that region. There is a strong propensity rule in the vibrational spectra of methanol for conservation of the torsional excitation,[18] which, under jet conditions, implies that only the lowest torsional state of each

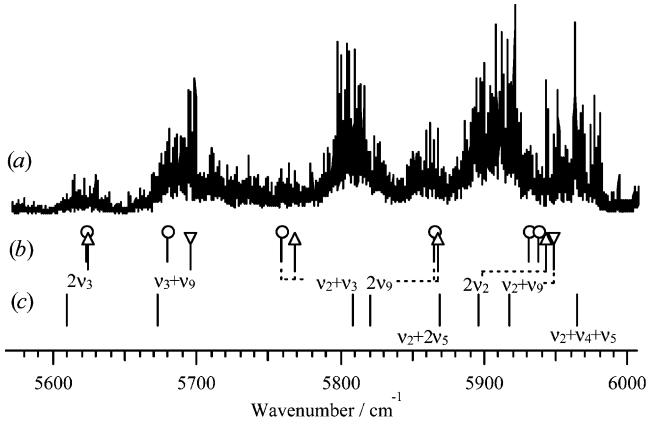

Figure 9. (a) IRLAPS spectrum of jet-cooled methanol in the $\upsilon_{CH} = 2$ region (ref 13). (b) Calculated transition wavenumbers (this work, fully coupled) including interactions of the torsion with the CH stretch but neglecting stretch−bend interactions. Upper state torsion−vibration symmetries are labeled as A_1 (△), A_2 (▽), and E (○). (c) Calculated transition wavenumbers (ref 17) including CH stretch−bend interactions but neglecting torsional motion. The band assignments are those given in ref 17, and dotted lines connect them with the closest features in trace (b) having the required symmetry.

distinct CH stretch vibration will appear with significant intensity in the spectrum. The agreement (Figure 9) of our calculated CH stretch frequencies for the two lowest bands in the $\upsilon_{CH} = 2$ region is excellent because these two vibrations are anharmonically shifted out of resonance with the CH stretch−bend interaction. The agreement is poor in the higher part of the polyad where the CH stretch−bend interaction is on resonance. There are a total of 18 stretch−bend combination states in this region, of which Hänninen and Halonen only reported the frequencies of the two that they calculated to be most intense. Another source of model error in the higher part of the $\upsilon_{CH} = 2$ polyad arises from our neglect of the stretch−bend coupling in the fundamental region, which leads to consequent error in the determination of λ. The local-mode overtones appearing in Figure 1 are not sensitive to λ, but the higher vibrations in each polyad are dominantly local−local in character and therefore depend on λ. Firm spectroscopic assignments and a detailed understanding of the $\upsilon_{CH} = 2$ region will have to wait until high-resolution spectra are available.

For $\upsilon_{CH} = 3$ and higher, the CH stretch−bend interaction is out of resonance with the local CH stretch features that appear in the spectra, and the observed bands appear at the frequencies expected for the local-mode overtones (Figure 1). However, we still see the effects of vibrational interactions with modes other than the four included in the model. The IRLAPS spectra for $\upsilon_{CH} = 3$ and higher contain only the broad unstructured bands characteristic of rapid IVR (100 fs $\leq \tau_{IVR} \leq$ 1 ps).[13] This means that, for the higher CH overtones, the present model can, at best, describe the short-time behavior. Because the model derives from low-resolution information, specifically the well-resolved splitting of the ν_a and ν_b overtones (Figure 1), there is reason to expect the model to be qualitatively valid at short times.

D. Comparison to Other Molecular Systems. The question of diabatic vs adiabatic separation of nuclear degrees of freedom has been addressed, at least implicitly, in other circumstances. In the statistical adiabatic channel model of chemical reactions,[19,20] each of the adiabatic modes is treated as individually adiabatic and separable from all other modes, including from the other adiabatic modes. That is, the quantum numbers for each adiabatic vibration are treated as good quantum numbers, and the adiabatic channel potential curves for different excitations of the adiabatically "conserved" modes may cross.[19] Thus, the adiabatic channel model provides a sort of precedent for what, in this paper, we have called diabatic potential curves.

A much more closely related example is the treatment of the CH stretch overtones of nitromethane by Cavagnat and Lespade[21] in which they treat explicitly the coupling of the CH stretch with internal rotation. In Figure 9 of ref 21, they show that the effective torsional potential of nitromethane is transformed from a low (2 cm^{-1}) 6-fold barrier for $\upsilon_{CH} = 0$ to a much higher 2-fold barrier for $\upsilon_{CH} = 6$. For the lower levels $\upsilon_{CH} = 0-3$, they use a normal-mode description of the CH stretches and separate them adiabatically from the internal rotation. However for $\upsilon_{CH} = 4-6$, they treat the CH stretches as local modes with the CH amplitude constrained to lie on a single CH bond. That excited CH bond, now distinguishable from the other two CH bonds, may come into alignment with each of the two oxygens of the nitro group to give rise to the 2-fold effective torsional potential shown in their Figure 9. However, there are three equivalent 2-fold torsional potentials at $\upsilon_{CH} = 6$ separated by 120°, one for excitation of each of the three methyl hydrogens. These three potentials cross at several places, so that we would call them diabatic potentials. The transition from adiabatic to diabatic behavior in their calculation occurs at $\upsilon_{CH} = 4$, the same level at which we have found the transition in methanol.

IV. Conclusions

The model calculation presented here shows a qualitative change in the torsion−vibration dynamics of methanol as the CH stretch is excited to high overtones. The adiabatic behavior (G_6 symmetry) of the CH fundamentals is replaced in the high overtone region by approximate diabatic behavior. There, the three identical diabatic potentials each have C_s symmetry ($3\times C_s$), giving systematic 3-fold degeneracies. In every CH stretch polyad, the highly excited torsion approaches free internal rotation ($C_{\infty v}$) and decouples from the CH stretch vibrations. For $\upsilon_{CH} = 1$, the CH stretches become the $A_1 + E$ normal modes expected in a C_{3v} symmetric rotor to give the overall approximate symmetry $C_{3v}\otimes C_{\infty v}$ with 2- and 4-fold degeneracies. For the higher polyads, the CH stretches become three equivalent local CH vibrations with approximate symmetry $3\times C_{\infty v}$ and systematic 6-fold degeneracies.

Acknowledgment. The author wishes to thank Trocia Clasp and Michael Kellman for helpful discussions. The work was supported by the Division of Chemical Sciences, Offices of Basic Energy Sciences, Office of Energy Research, U.S. Department of Energy under Grant No. DE-FG02-90ER14151. Support of this work does not constitute endorsement by the DOE of views expressed in this paper.

References and Notes

(1) Bunker, P. R.; Jensen, P. *Molecular Symmetry and Spectroscopy*, 2nd ed.; NRC Research Press: Ottawa 1998.
(2) Hougen, J. T. *J. Mol. Spectrosc.* **1997**, *181*, 287.
(3) Fehrensen, B.; Luckhaus, D.; Quack, M.; Willeke, M.; Rizzo, T. R. *J. Chem. Phys.* **2003**, *119*, 5534−44.
(4) Wang, X.; Perry, D. S. *J. Chem. Phys.* **1998**, *109*, 10795−10805.
(5) Xu, L.-H.; Wang, X.; Cronin, T. J.; Perry, D. S.; Fraser, G. T.; Pine, A. S. *J. Mol. Spectrosc.* **1997**, *185*, 158−172.
(6) Lees, R. M.; Mollabashi, M.; Xu, L.-H.; Lock, M.; Winnewisser, B. P. *Phys. Rev. A: At., Mol., Opt. Phys.* **2002**, *65*, 042511/1−042511/7.
(7) Lees, R. M.; Xu, L.-H. *Phys. Rev. Lett.* **2000**, *84*, 3815−3818.
(8) Lees, R. M.; Xu, L.-H.; Johns, J. W. C.; Lu, Z. F.; Winnewisser, B. P.; Lock, M.; Sams, R. L. *J. Mol. Spectrosc.* **2004**, *228*, 528−543.

(9) Lees, R. M.; Xu, L.-H.; Kristoffersen, A. K.; Lock, M.; Winnewisser, B. P.; Johns, J. W. C. *Can. J. Phys.* **2001**, *79*, 435−447.

(10) Clasp, T. N.; Perry, D. S. *J. Chem. Phys.* **2006**, *125*, 104313/1−104313/9.

(11) Kellman, M. E.; Tyng, V. *Acc. Chem. Res.* **2007**, *40*, 243−250.

(12) Tyng, V.; Kellman, M. E. *J. Phys. Chem. B* **2006**, *110*, 18859−18871.

(13) Rueda, D.; Boyarkin Oleg, V.; Rizzo Thomas, R.; Chirokolava, A.; Perry David, S. *J. Chem. Phys.* **2005**, *122*, 44314.

(14) Fang, H. L.; Meister, D. M.; Swofford, R. L. *J. Phys. Chem.* **1984**, *88*, 405−409.

(15) Child, M. S.; Halonen, L. In *Advances in Chemical Physics*; Rice, I. P. a. S. A., Ed.; Interscience Publishers: New York, 1984; Vol. LVII, pp 1−58.

(16) Watson, I. A.; Henry, B. R.; Ross, I. G. *Spectrochim. Acta, Part A* **1981**, *37*, 857−865.

(17) Hänninen, V.; Halonen, L. *Mol. Phys.* **2003**, *101*, 2907−2916.

(18) Rueda, D.; Boyarkin, O. V.; Rizzo, T. R.; Mukhopadhyay, I.; Perry, D. S. *J. Chem. Phys.* **2002**, *116*, 91−100.

(19) Quack, M.; Troe, J. In *Encyclopedia of Computational Chemistry*; Schleyer, P. v. R., Ed.; Wiley: New York, 1998; Vol. 4, pp 2708−2726.

(20) Quack, M.; Troe, J. *Ber. Bunsen.−Phys. Chem.* **1974**, *78*, 240−52.

(21) Cavagnat, D.; Lespade, L. *J. Chem. Phys.* **1997**, *106*, 7946−7957.

(22) Xu, L.-H.; Hougen, J. T. *J. Mol. Spectrosc.* **1995**, *169*, 396−409.